Cancer Cell International

RESEARCH

Open Access

Machine learning and single-cell RNA sequencing reveal relationship between intratumor CD8+ T cells and uveal melanoma metastasis

Shuming Chen[1,2†], Zichun Tang[1,2†], Qiaoqian Wan[3], Weidi Huang[1,2], Xie Li[1,2], Xixuan Huang[1,2], Shuyan Zheng[1,2], Caiyang Lu[4], Jinzheng Wu[5], Zhuo Li[1,6*] and Xiao Liu[1,2*]

Abstract

Purpose Uveal melanoma (UM) is adults' most common primary intraocular malignant tumor. It has been observed that 40% of patients experience distant metastasis during subsequent treatment. While there exist multigene models developed using machine learning methods to assess metastasis and prognosis, the immune microenvironment's specific mechanisms influencing the tumor microenvironment have not been clarified. Single-cell transcriptome sequencing can accurately identify different types of cells in a tissue for precise analysis. This study aims to develop a model with fewer genes to evaluate metastasis risk in UM patients and provide a theoretical basis for UM immunotherapy.

Methods RNA-seq data and clinical information from 79 μm patients from TCGA were used to construct prognostic models. Mechanisms were probed using two single-cell datasets derived from the GEO database. After screening for metastasis-related genes, enrichment analysis was performed using GO and KEGG. Prognostic genes were screened using log-rank test and one-way Cox regression, and prognostic models were established using LASSO regression analysis and multifactor Cox regression analysis. The TCGA-UVM dataset was used as internal validation and dataset GSE22138 as external validation data. A time-dependent subject work characteristic curve (time-ROC) was established to assess the predictive ability of the model. Subsequently, dimensionality reduction, clustering, pseudo-temporal analysis and cellular communication analysis were performed on GSE138665 and GSE139829 to explore the underlying mechanisms involved. Cellular experiments were also used to validate the relevant findings.

Results Based on clinical characteristics and RNA-seq transcriptomic data from 79 samples in the TCGA-UVM cohort, 247 metastasis-related genes were identified. Survival models for three genes (SLC25A38, EDNRB, and LURAP1) were

†Shuming Chen and Zichun Tang Co-first authors.

Xiao Liu and Zhuo Li are co-corresponding authors.

*Correspondence:
Zhuo Li
LiZhuo75@csu.edu.cn
Xiao Liu
Liuxiao8@csu.edu.cn

Full list of author information is available at the end of the article

then constructed using lasso regression and multifactorial cox regression. Kaplan-Meier survival analysis showed that the high-risk group was associated with poorer overall survival (OS) and metastasis-free survival (MFS) in UM patients. Time-dependent ROC curves demonstrated high predictive performance in 6 m, 18 m, and 30 m prognostic models. Cell scratch assay showed that the 24 h and 48 h migration rates of cells with reduced expression of the three genes were significantly higher than those of the si-NC group. CD8 + T cells may play an important role in tumour metastasis as revealed by immune infiltration analysis. An increase in the percentage of cytotoxic CD8 + T cells in the metastatic high-risk group was found in the exploration of single-cell transcriptome data. The communication intensity of cytotoxic CD8 was significantly enhanced. It was also found that the CD8 + T cells in the two groups were in different states, although the number of CD8 + T cells in the high-risk group increased, they were mostly in the exhausted and undifferentiated state, while in the low-risk group, the CD8 + T cells were mostly in the functional state.

Conclusions We developed a precise and stable 3-gene model to predict the metastatic risk and prognosis of patients. CD8 + T cells exhaustion in the tumor microenvironment play a crucial role in UM metastasis.

Keywords Uveal melanoma, Prognostic models, Immune microenvironment, Tumour metastasis

Introduction

Uveal melanoma (UM) is the most common primary intraocular malignant tumor in adults [1]. Primary UM can be treated with either radiation or surgery and has a low- local recurrence rate. However, distant metastases, which often occur in the liver, are present in approximately 40% of patients during the subsequent course and the mortality rate for the population is high, up to 50% within a period of 4 to 5 years [2–4]. There is no effective treatment available for metastatic melanoma, which is why it is critical to identify and screen patients who are at high risk of developing metastases.

Previous studies have been conducted to predict the risk of UM metastasis by clinicopathological features, chromosomal features and gene expression profiles (GEP) [5]. Certain clinicopathological features such as tumor thickness, peripheral location, patient age, vision loss, and ocular melanocytosis can be used to assess the risk of metastasis in UM [6,7]. These data are most readily available in clinical work but are slightly less accurate in assessing metastasis and prognosis. With the development of chromosomal and genetic testing methods, chromosomal abnormalities such as monosomy 3 and GEP analysis have shown superior predictive accuracy over clinicopathological features 8,98,9. An increasing number of genes have been used in recent studies to predict the risk of metastasis in UM, for example, PRAME (preferentially expressed antigen in melanoma) [10], estrogen receptors (ERs) [11], SLC25A38 [9], PRRX1 [12], etc.

Several multigene models have been developed using machine learning methods to assess the metastasis and prognosis of UM. The prediction model developed by Onken et al., based on gene expression profiling (GEP), demonstrated good accuracy and stability [13,14]. These models have high accuracy and robustness. However, each model included more than 10 genes to improve accuracy, leading to higher genetic testing costs, limiting their large-scale clinical application. Additionally, the specific mechanisms by which the genes in the models affect UM metastasis have not been fully elaborated upon. As a result, these models can only predict the risk of UM metastasis and cannot provide a specific protocol to prevent it.

The unique tumor microenvironment results from the eye's immune-privileged environment [15]. A study comparing immune infiltration in all tumors in TCGA revealed that UM had the lowest level of immune infiltration [16]. As a result, previous studies of metastatic mechanisms in UM have tended to focus on tumor heterogeneity. Some UM cells lack immunogenicity, which may contribute to the high risk of UM metastases [17]. However, the role played by immune cells in the tumor microenvironment is still unclear. The main types of immune cells infiltrating UM are T cells and macrophages [18]. Our study aimed to explore the function of these immune cells preliminarily.

The model mentioned above was based on bulk transcriptome sequencing data, which is easily accessible. However, it cannot accurately distinguish between different types of cells in tumor tissues, making it difficult to understand how the immune microenvironment affects tumor metastasis. In contrast, single-cell transcriptome sequencing data is more expensive, but the sequencing accuracy is extremely high. It can differentiate between various types of cells in the tissue for analysis. As a result, single-cell transcriptome sequencing technology has significantly advanced the understanding of many disease mechanisms in recent years [19–21].

Our study aims to develop a new model with fewer genes to improve the applicability of GEP analysis in clinical work. We also investigated the metastatic mechanism of UM using single-cell transcriptome sequencing data. The study builds a practical model and explores specific mechanisms in UM metastasis. It can be used in clinical work to assess the risk of UM metastasis and provide a theoretical basis for UM immunotherapy.

Methods

Data resources and workflow

Data for constructing and validating prognostic models were obtained from the TCGA and GEO databases. The TCGA-UVM dataset was used to construct the prognostic models and contains bulk RNA-seq data and clinical information for 80 μm patients. Another cohort GSE22138 include 63 μm patients were chosen from the GEO database (https://www.ncbi.nlm.nih.gov/geo/). Baseline clinicopathological information, metastatic status, and final clinical outcome were recorded for each patient. The two single-cell transcriptome sequencing datasets used to probe mechanisms were obtained from the GEO database. The single-cell dataset GSE138665 contains tumor single-cell transcriptome data from 6 primary UM patients. The single-cell database GSE139829 contains tumor single-cell transcriptome data from 8 primary UM patients. The flowchart of this study is showed in the Fig. 1.

Metastasis related genes identification and functional enrichment analysis

After removing the 1 sample with missing transfer status, the remaining 79 samples from the TCGA-UVM dataset were divided into two subgroups according to transfer status, and subsequently the R packages "DESeq2", "edgeR" and "limma" to assess the differential mRNA expression between the metastatic and non-metastatic groups. The criteria for selecting metastasis related genes (MRGs) included |log2(fold change)| > Mean [log2(fold change)] + 2SD[log2(fold change)]and a false discovery rate (FDR)-adjusted $p<0.05$.The MRGs that were co-upregulated or co-downregulated in the three R packages were considered to be metastasis-associated genes. The results were visualized using the R packages "ggplot2" and "MetaVolcanoR".

To explore potential biological processes related to the obtained MRGs, we performed gene ontology (GO) and Kyoto Encyclopedia of Genes and Genomes (KEGG) enrichment analysis using the R package "clusterProfifiler". The GO enrichment analysis was conducted based on three aspects including biological process (BP), molecular functions (MF) and cellular components (CC). The results were visualized using R packages "ggplot2" and "BioEnricher".

Survival analysis and prognostic modeling

Survival was estimated by the Kaplan-Meier method using MGRs, and any differences in survival were evaluated with log-rank test and univariate Cox regression. Genes with p-values < 0.05 for both tests were considered to be associated with prognosis. Least absolute shrinkage and selection operator (LASSO) regression analysis was then performed using the R package "glmnet" to avoid overfitting. Subsequently, multivariate Cox regression analysis (significance level: $p<0.05$) was performed to establish a prognostic model. According to the corresponding regression coefficient calculated by multivariate Cox regression analysis, the risk score can be calculated. The risk score was computed as follow:

$$\mathrm{Riskscore} = \sum_{i=0}^{n} (Coef_i \times Exp_i)$$

$\mathrm{Coef_i}$ is the corresponding regression coefficient calculated by multivariate Cox regression analysis and $\mathrm{Exp_i}$ is the expression value of the genes selected by multivariate Cox regression analysis.

Evaluation of prognostic model

The TCGA-UVM dataset was used as the internal validation dataset GSE22138 was used as the external validation dataset, and the samples were divided into high-risk and low- risk groups according to the survival model, respectively. Kaplan-Meier survival analyses were performed using the R packages "survival" and "survminer" to compare the OS and MFS between different groups. R package "timeROC" were used to establish time-dependent receiver operating characteristic curves (time-ROC) to evaluate the predictive power of the model. The larger the area under the curve (AUC), the stronger the predictive ability of the risk model.

Cell culture

The human UM cell line MuM-2B were purchased from iCell Bioscience Inc. (iCELL-h148; Shanghai, China). Cells were cultured in RPMI- 1640 medium (Gibco, USA) supplemented with 10% FBS (Gibco, USA) and 1% penicillin–streptomycin in an incubator containing 5% CO2 at 37 °C. The cell experiments were performed in the logarithmic growth period.

Quantitative real-time PCR

Total RNA from MUM2B cells were extracted using the SteadyPure Quick RNA Extraction kit (AG21023; Accurate Biotechnology, Beijing, China). And the reverse-transcribed using EVo M-MLV RT Mix Kit with gDNA Clean for gPCR Ver.2 (AG11728; Accurate Biotechnology, Beijing, China) for qPCR. The resulting cDNAs were used for PCR using the SYBR® Green Premix Pro Taq HS qPCR Kit (Rox Plus) (AG11718-S, Accurate Biotechnology, Hunan). qPCR was performed using the StepOne Real-Time PCR system (4376 600; Applied Biosystems, Carlsbad, CA, USA). The PCR program was as follows: pre-denaturation at 95°C for 30 s, and 40 cycles of 5 s at 95°C and30 s at 60°C. The following primer sequences (all 5′ to 3′) were used for quantita-tive real-time PCR: EDNRD Forward: 5'- CCATTGGCCATCACTGCATT

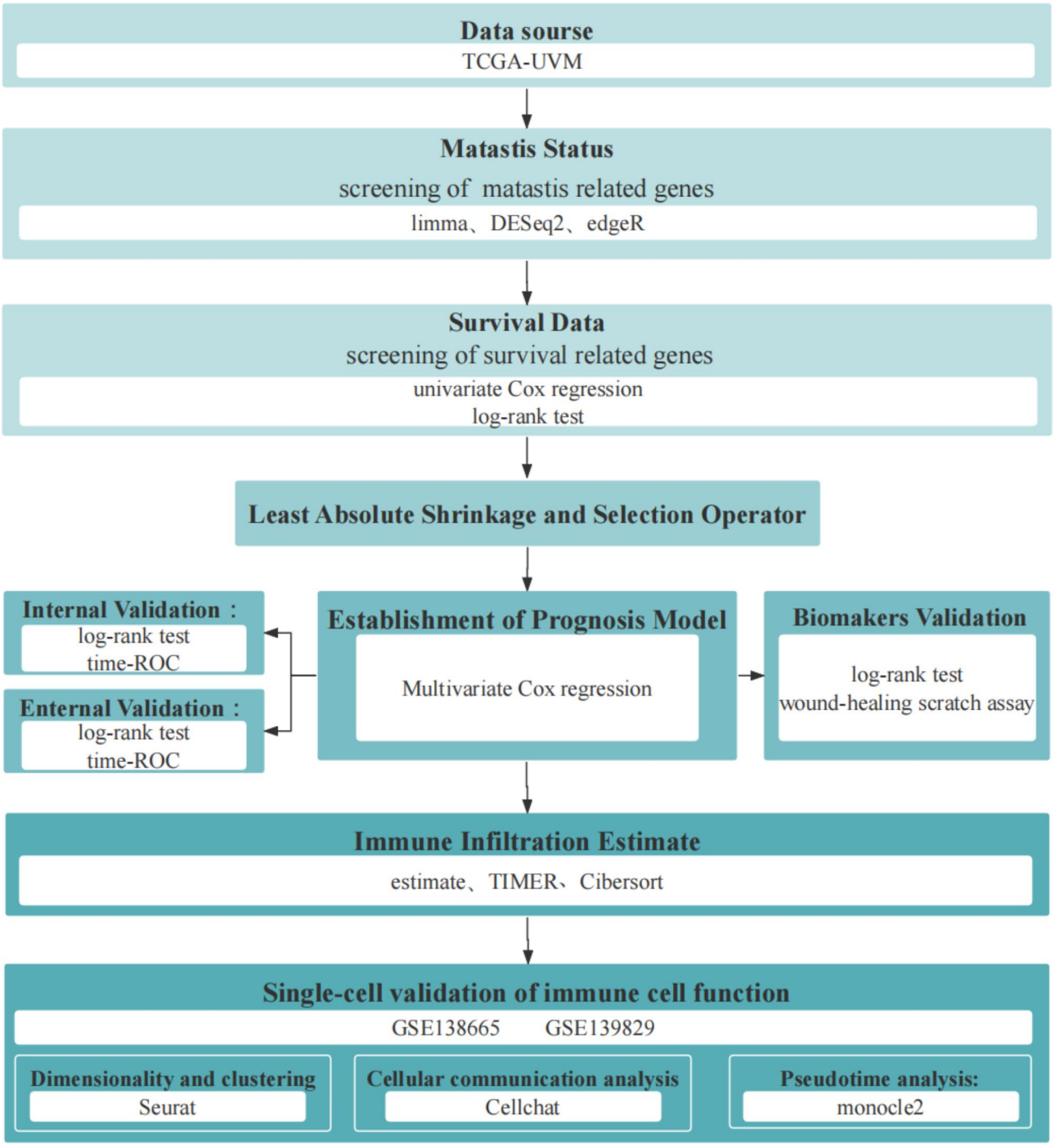

Fig. 1 Flowchart of this study

T −3′, Reverse: 5′-:CCGTCTCTGCTTTAGGTGATCAT −3′; LURAP Forward: 5′- CATGGAAACCTGGCTCATC A −3′, Reverse: 5′-GCTCTCTATCTTGGGTAACAGCA −3′, SLC25A38 Forward: 5′- GGGTCTCCTTGGGTATG TTCTT −3′, Reverse: 5′- CTCCTCTCCTCACATCCAG TCTT −3′, All data were normalized against endogenous glyceraldehyde 3-phosphate dehydrogenase (GAPDH) controls of each. sample Relative expressionwas calculated using the $2-\Delta\Delta CT$ method. Five biological replicates were included for each assay with three technical repli-cates for each biological replicate.

Transfection experiment

The siRNA mimics (si- NC, si-EDNRB, si-LURAP1, si-SLC25A38) and negative control (si-NC) were transfected into MUM-2B cells using a RiboFECT™ CP

Transfection Kit (RiboFECT CP, Guangzhou, China), Transfection was carried out according to the manufacturer's instructions.

Wound healing assay

MUM2B cells were seeded into 6-well plates with a density of 1.0×10^5 cells per well, and they adhered to the wall of the dish after incubating for 24 h. As described above, add corresponding transfection kit when reagent the density of the cells grows to between 30%~50%. When cells were cultured until 100% confluence, a straight line was scratched with a sterile pipette tip and the cells originally in the area of the line were removed. The medium was then refreshed with the medium. Samples were taken at the time points of 0, 24 and 48 h after scratching. Images were captured under a microscope at ×5 magnification.

Cell viability assay

Cell viability was evaluated by a CCK-8 kit (DOJINDO, Japen) according to the manufacturer's protocol. The ratio of cell viability was calculated as Atreat/Acontrol× 100%.

Apoptosis assay

Cell apoptosis was determined with an AnnexinV-Alexa Fluor 647/Pi kit (FXP023, 4 A Bio tech, Suzhou, China). Briefly, cells were seeded in 6-well plates (1×10^5/well). Transfection was carried out as described previously. After incubation with transfection kit for 48 ~ 72 h, cells were harvest and resuspended with 500 µl 1× binding buffer. 5 µL of Annexin V-FITC was added into the cells suspension, and 5 µL of PI was added to mix by gentle pipetting. The samples were analyzed with DxP Athena cell analyzer (Cytek Biosciences, USA). The data analysis was performed using Flow-Jo software.

Tumor microenvironment analysis

In order to quantify Immune cell infiltration, the R package "estimate" was first used to calculate the immunity score, stromal score and estimate score for each sample [22]. The scores of the various immune cells in each sample were then calculated using "TIMER" [23, 24]. Afterwards, we verified the above results with the R package Cibersort. Finally, the R package "corrplot" was used to calculate the correlation between the various immunization scores and the risk scores.

Single-cell transcriptome data quality control and integration

For each single-cell sequencing sample first screen the cells according to the follow-ing criteria:1) unique molecular identifier (UMI) > 400; 2) 100 < genes detected per cell < 8000; 3) percentage of mitochondrial genes < 10%; and 4) complexity ($\log_{UMI}$ (genes detected per cell)) > 0.8. Then the R package "DoubletFinder" was used to remove double cells. Finally, the R package "harmony" was used to remove the batch effect between samples to complete the data integration.

Dimensionality reduction and clustering

The integrated data were analyzed for dimensionality reduction and clustering analysis using the R package "Seurat". First, the Log-Normalize and ScaleData function are applied to the filtered and integrated data. The Find Variable Feature function was used to filter out the top 2000 highly variable genes for further analysis by principal component analysis (PCA); the percentage change between each principal component (PC) and subsequent components was calculated. If the percentage is less than 5%, the current PC number is selected for subsequent analysis. Then dimensionality reduction analysis is performed using the t-Distributed Stochastic Neighbor Embedding (tSNE) algorithms, and finally cluster analysis was analyzed using the FindClusters function. Cell types were annotated based on marker genes expression. The markers used were as follow-s: tumor cells (MLANA, MITF), immune cell (PTPRC), T cells (CD3D, CD3E), T cells subset: cytotoxic CD8 + T (CD8A, PRF1, GZMA, GZMK, NKG7), native T cells (IL7R), T regulatory cells (FOXP3, TNFRSF4, IKZF2, IL2RA), natural killer cells (GNLY, TRDC), myeloid cells (CSF1R), myeloid cells subset: macrophages(CD163), mitotic macrophages (MKI67), M2 macrophages (C1QA, C1QB, C1QC, IL10), M1 macrophages (C1QA, C1QB, C1QC, lackof M2 macrophage markers), monocytes (VCAN, FCN1, CD300E, S100A12, EREG, STXBP2, ASGR1), dendritic cells (CD1C), fibroblasts (MGP), microglial cells (FTL, APOC1), astrocyte (CCL2, GADD45B), Schwann cells (S100A1, CRYAB), neural progenitor cells (STMN1, UBE2C, TUBA1B), melanocytes (TYRP1, PMEL), Photoreceptor cells (RCVRN).

Afterwards, the risk score of each sample was calculated by the survival model described above, and the samples were categorized into high-risk and low-risk groups based on the risk score for downstream analyses.

Cellular communication analysis

In order to investigate the communication between various types of cells in the UM microenvironment, we used the R package "CellChat" for Cellular communication analysis. The Seurat objects were first divided into two groups, high risk and low risk, leaving the cell types that were present in both groups, then the Seurat objects were converted to CellChat objects, and finally cellular communication was analyzed for both groups using the default parameters. Use mergeCellChat function to integrate the data of the two groups.

Pseudotime analysis

We used a subset of cytotoxic CD8+T cells from Seurat objects for the proposed time analysis. Cytotoxic CD8+T cells were first analyzed by Dimensionality reduction and clustering according to the above methods. Use the FindAllmarker function to find the marker genes for each subset and annotate these subsets using these marker genes. T cell exhaustion markers derived from previous studies [25]: progenitor states 1 (Tex_prog1):SLAMF6+CD69+, progenitor states 2 (Tex_prog2): SLAMF6+CD69–, "effector-like" cells (Tex_int): SLAMF6–CD69–,terminally exhausted (Tex_term): SLAMF6–CD69+.Then the R package "monocle2" was used to perform the pseudotime analysis and calculate the pseudotime value for each cell. The starting point of differentiation is then inferred using the R package "CytoTRACE" [26]. The BEAM function was used to infer key regulatory genes during differentiation. The metacell transition expression matrix was constructed using the R package hdWGCNA. Subsequently, the correlation between differentiation-related genes and risk genes was assessed using the R package corrplot.

Results

Identify metastasis related genes

Based on the metastasis status, UM patients from TCGA were divided into two groups (61 patients without metastasis, and 18 patients with metastasis). The clinical baseline information of these patients can be found in the Additional file1 Supplementary Table 1. There were and 499 down-regulated genes 142 up-regulated genes in metastatic UM tumors were calculated by DESeq2, 503 down-regulated genes and 162 up-regulated genes calculated by edgeR; And 350 down-regulated genes and 363 up-regulated genes calculated by limma (Fig. 2A). The overlapping genes (176 down-regulated genes, 71 up-regulated genes and totally 247 genes) were considered to be MRGs (Fig. 2A, B). The GO pathway of enrichment analysis reveals that the MRGs are mainly enriched in pathways associated with the matrix microenvironment and

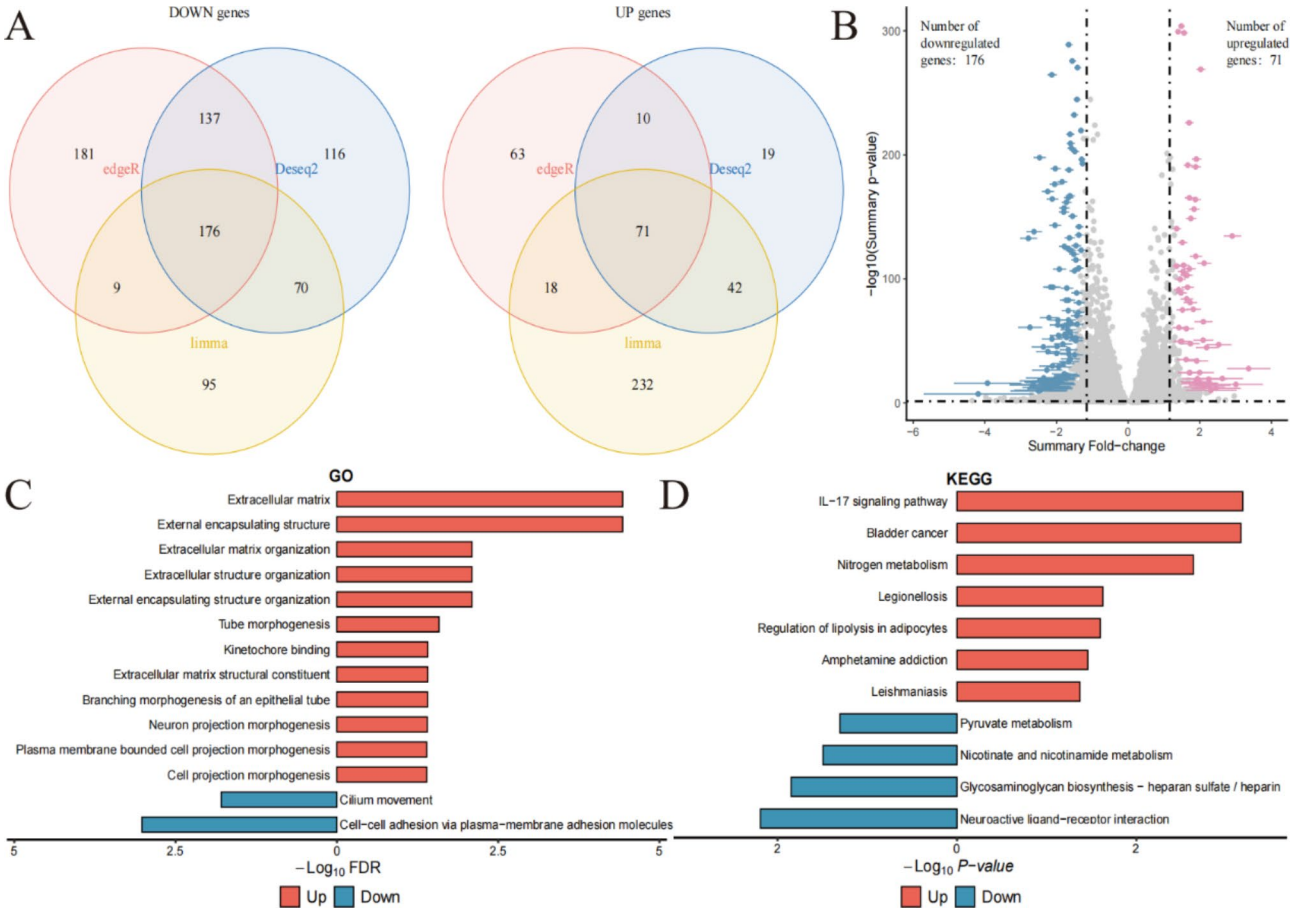

Fig. 2 Metastasis related genes identification and functional enrichment analysis. **A**) Venn plot showing the number of up- and down-regulated metastasis-related genes calculated by the three methods (edgeR, Deseq2 and limma). **B**) Total number of genes with significant changes in expression. Among the significantly differentially expressed genes,71 and 176 genes were up-regulated (red dots) and down-regulated (blue dots), respectively. **C**) Gene ontology (GO) functional annotation of the metastasis-related genes. **D**) Kyoto Encyclopedia of Genes and Genomes (KEGG) functional annotation of the metastasis-related genes

cell movement (Fig. 2C). The KEGG pathway of enrichment analysis reveals that these genes are associated with the IL-17 pathway and the metabolism (Fig. 2D).

Establish and evaluation the prognostic modeling

127 genes were significantly related to OS of UM patients calculated by log-rank test ($p<0.05$) and 143 genes were significantly related to OS of uveal melanoma patients calculated by Cox regression($p<0.05$). The overlapping 117 genes were considered to be related to prognostic of UM patients. The overlapping genes were included in the LASSO regression analysis to avoid overfitting problems in the risk signature. We used 10-fold cross-validation to filter for characterized genes corresponding to the smallest lambda value (Fig. 3A, B). The multivariate Cox regression analysis was applied to the genes returned from the LASSO regression analysis (5 genes) to construct the prognostic model, which included three genes (SLC25A38, EDNRB and LURAP1). All of these genes are protective factors for the survival of UM patients (Fig. 3C).

The risk scores were calculated based on models constructed by the multivariate Cox regression analysis. Kaplan-Meier survival analyses showed that patients in the low- risk group had a more likely to have better OS (Fig. 3D) and MFS (Fig. 3E). We then compared the OS/MFS and the expression of diagnostic biomarkers between the two groups. Our results revealed that patients with low- risk score had a high-survival rate and high-expression of diagnostic biomarkers (Fig. 3F, G). In addition, we evaluated the AUC values in two independent cohorts and showed that risk score were highly accurate in predicting 6, 18, and 30 months prognosis in patients with UM (Fig. 3H, I).

Diagnostic biomarkers prevent tumor cell migration

We explored the effects of the genes alone in the models. OS of samples in TCGA-UVM cohort was significantly higher in the group with higher SLC25A38, EDNRB and

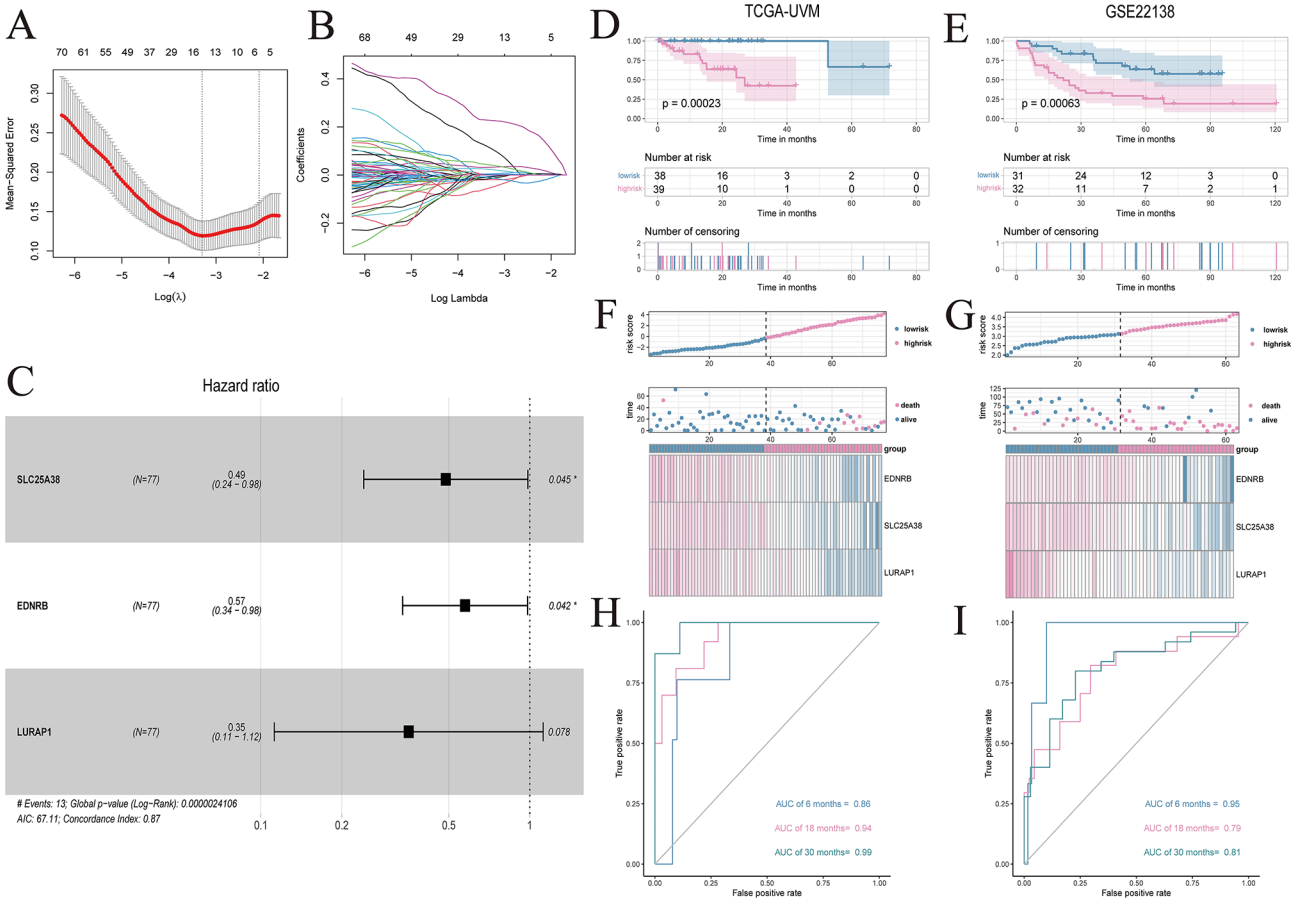

Fig. 3 Establish and evaluation the prognostic modeling. **A** and **B**) The feature genes corresponding to the minimum value of lambda in LASSO regression. **C**) Forest plot showing multifactor Cox regression prognostic model. **D**) Overall survival in the low– and high- risk group patients in TCGA-UVM cohorts. **E**) Metastasis-free survival in the low– and high-risk group patients in GSE22138 cohorts. **F** and **G**) Distribution of risk score and diagnostic biomarkers expression according to the survival status and time in TCGA-UVM (**F**) and GSE22138 cohorts (**G**). **H** and **I**) Receiver operator characteristic (ROC) analysis of prognostic model in TCGA-UVM (**H**) and GSE22138 cohorts (**I**)

LURAP1 expression (Fig. 4A). The same result is found in the GSE22138 cohort. Higher SLC25A38, EDNRB and LURAP1 expression groups have higher MFS (Fig. 4B). The relative mRNA levels of si-EDNRB, si-LURAP, and si-SLA25A38 that differed most from those of si-NC were si-EDNRB1, si-LURAP1, and si-SLA25A381 (see Additional file Figure S1 A ~ C).The results of the scratch assay showed that the migration rate of cells transfected with si-EDNRB, si-LURAP1 and si-SLC25A38 was significantly increased compared with the si-NC group at 24 h (Fig. 4C, D), and that the migration rate of the si-LURAP1 and si-SLC25A38 groups was significantly higher than that of the si-NC group at 48 h (Fig. 4C, E). Cell viability assay showed no significant differences between the si-LURAP1 group, the si-SCL25A38 group, the si-EDNRB group and the si-NC group (see Additional file Figure S1D). The results of apoptosis assay showed no significant difference in apoptosis between the four groups either (see Additional file Figure S1E).

Metastatic and prognostic features of UM correlate with immune infiltration

Afterwards, we calculated the immune infiltration in both groups, and the immune score, stromal score, and estimate score (which was negatively correlated with tumor purity) were significantly higher in the high-risk group than in the low- risk group (Fig. 5A). To further explore immune cell function, we calculated scores for 8 immune cells. CD8+ T cell scores were significantly higher and B cell scores and Myeloid DC scores were significantly low-er in the high-risk group than in the low- risk group (Fig. 5B). Then, we calculated the correlation between various immune scores and risk scores and found that risk scores were significantly and positively correlated with immune scores, stromal scores, and CD8+ T cell scores (Fig. 5C).We then calculated the CD8+T cell, B cell, and DC cell scores again using Cibersort and found that only the CD8+T cell score was significantly different between the two groups (Fig. 5D).Correlation analysis between Cibersort-calculated immunization scores and risk scores showed that CD8+T cell scores were significantly associated with risk scores(Fig. 5E).

Single-cell transcriptome sequencing data explore tumor microenvironment

After stringent filtering, we retained a total of 48,147 cells from 14 samples for subsequent analysis. A total of 10 cell types were identified after first dimensionality reduction and clustering analysis. Afterwards, T cells and myeloid cells were again analyzed by dimensionality reduction and clustering, and 21 cell types were finally identified (Fig. 6A, B). The proportion of cells of each cell type in each sample was then calculated (Fig. 6C). The risk scores for each sample were then calculated based on the previously established model and the samples were categorized into a high-risk portfolio low- risk group based on the average risk scores (Fig. 6D). The percentage of each type of cell in the two groups was then calculated and it was found that the percentage of tumor cells decreased and the percentage of cytotoxic CD8+T cells increased in the high-risk group (Fig. 6E). Finally, the expression of prognostic biomarkers was explored and found that SLC25A38 was more expressed in T cells and EDNRB and LURAP1 were more expressed in tumor cells (Fig. 6F-H).

CD8+T cells play an important role in cellular communication

We first compared the number and strength of total cellular communication within the both groups. The number and strength of cellular communications were higher in the high-risk group than in the low- risk group (Fig. 7A). Changes in the number and strength of communications of individual cell types were later compared between the two groups. There was a greater enhancement in the communication strength of cytotoxic CD8+ T cells in all cell types in the high-risk group (Fig. 7B). And both high-risk and low- risk groups cytotoxic CD8+T cells are very important in cellular communication (Fig. 7C). We then identified the pathways that differed between the two groups, with 42 significant pathways in the high-risk group and 11 significant pathways in the low- risk group (Fig. 7D). We then selected communications with a cellular communication probability greater than 0.1 and associated with cytotoxic CD8+ T cells and compared the expression of ligand receptors for these pathways between the two groups (Fig. 7E). Finally, 4 pathways were identified that were significantly expressed in the high-risk group for cytotoxic CD8+ T cell-tumor cell communication: the APP pathway, the MHC-I pathway, the CD99 pathway, and the MIF pathway, of which only the CD99 pathway was outgoing signaling in CD8+ T cells (Fig. 7F-I).

Exploring the differentiation trajectory of CD8+ T cells

To explore cytotoxic CD8+ T cells in depth, we subdivided 2650 cytotoxic CD8+T cells into 4 subsets and named these 4 subsets according to CD8+T cell exhaustion marker genes (Fig. 8A-C). We calculated the proposed times for these four subgroups and ordered them by CytoTRACE score (Fig. 8D). We found that Tex_prog1 were located at the beginning of differentiation and Tex_int and Tex_term were located at the end of differentiation (Fig. 8E). We compared cytotoxic CD8+ T cells differentiation between the two groups and found that cytotoxic CD8+T cells in the high-risk group were located at the beginning of differentiation (Fig. 8D). Afterwards, we calculated the proportion of T cells of

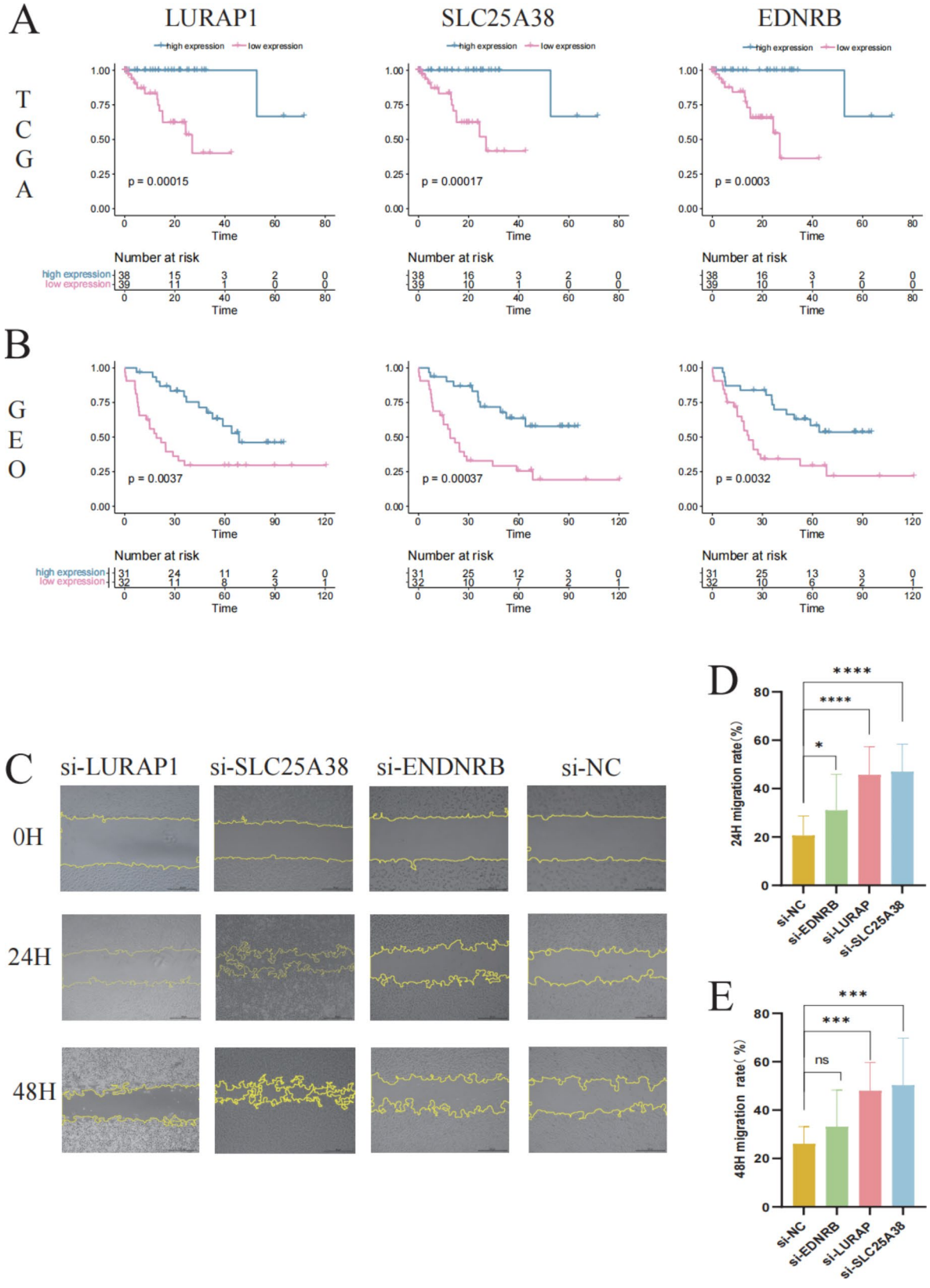

Fig. 4 Diagnostic biomarkers promote tumor cell migration. **A**) Overall survival in the low– and high- diagnostic biomarkers expression group patients in TCGA-UVM cohorts. **B**) Metastasis-free survival in the low- and high-diagnostic biomarkers expression group patients in GSE22138 cohorts. **C**) Wound healing assay was used to detect cell migration ability in si-LURAP, si-SLC25A38, si-EDNRB, si-NC UM cells. **D**) Quantitative analyses of wound healing assay in 24 h, $n=4$, *$p<0.05$, ****$p<0.0001$ one-way ANOVA. **E**) Quantitative analyses of wound healing assay in 48 h, ns $p>0.05$, ***$p<0.001$ one-way ANOVA

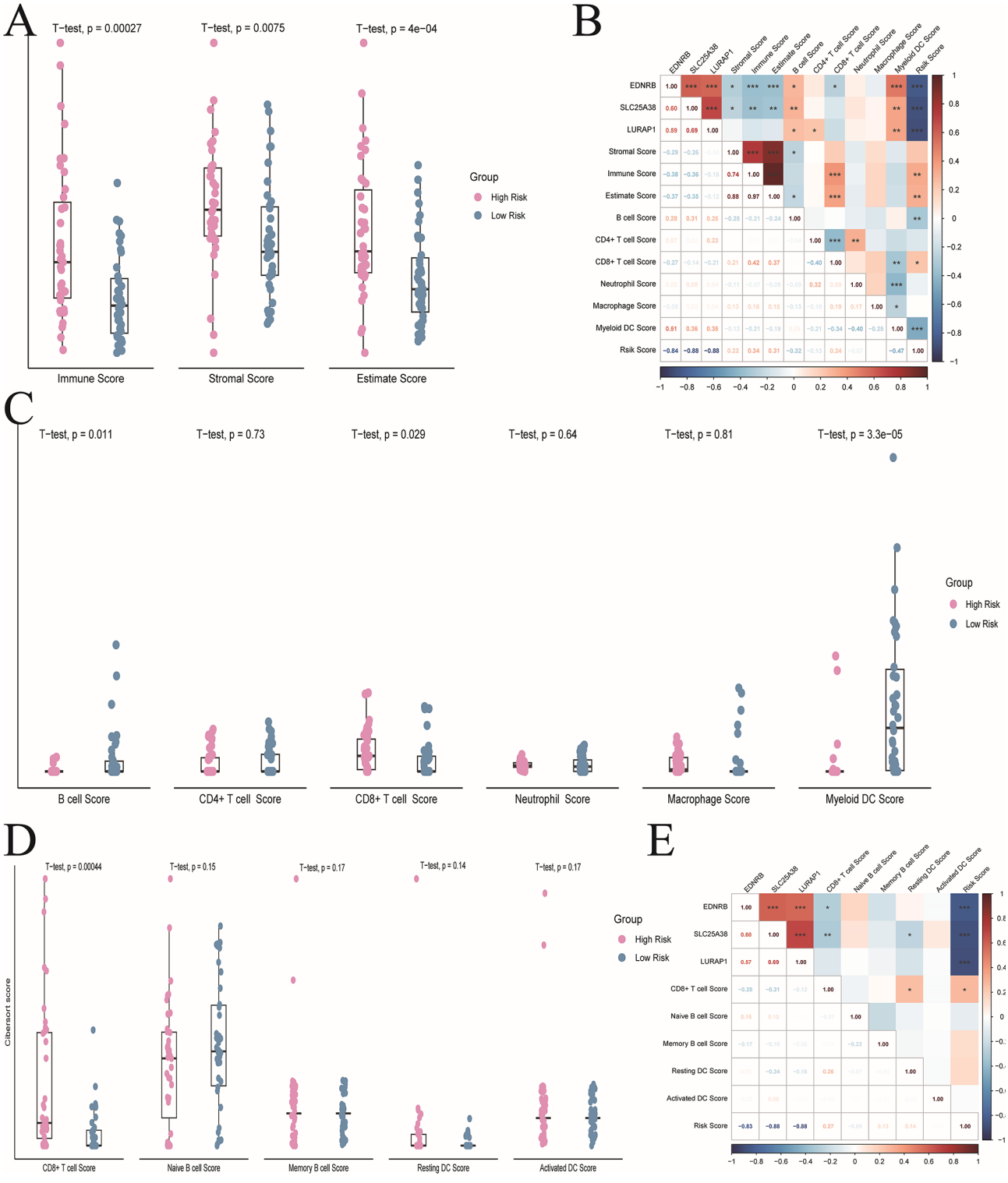

Fig. 5 Metastatic and prognostic features of UM correlate with immune infiltration **A**) Estimate analysis scores of low- and high-risk group. **B**) TIMER scores of low- and high- risk group. **C**) Heatmap of correlation between various estimate analysis scores and risk scores. **D**)Cibersort scores of low- and high- risk group. **E**)Heatmap of correlation between various Cibersort scores and risk scores

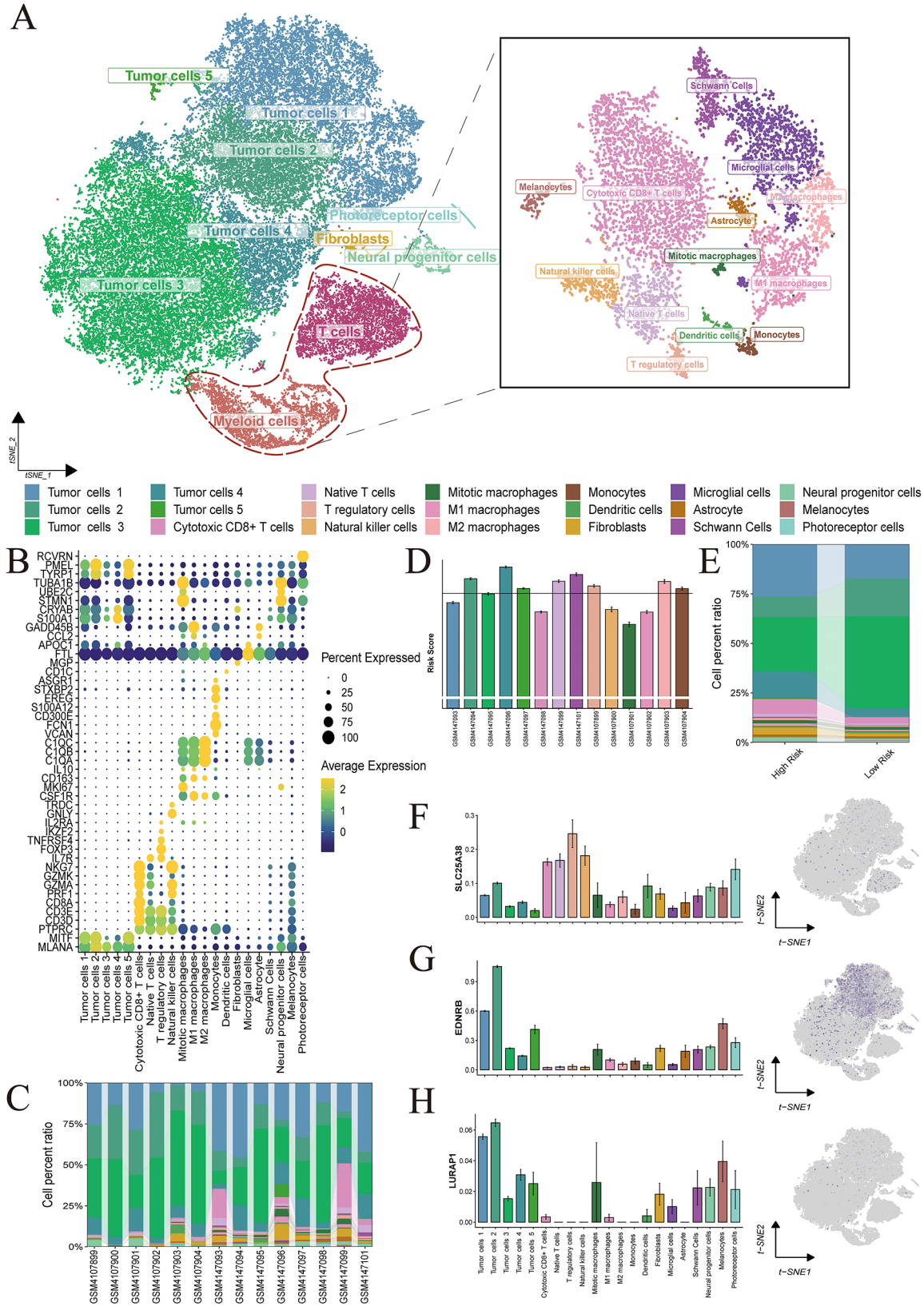

Fig. 6 Single-cell transcriptome sequencing data explore tumor microenvironment **A**) Clustering projection according to Seurat's clustering system using tSNE as the dimension reduction method. **B**) Bubble plot of marker genes. **C**) Stacked plots of the proportion of different cell types in each sample. **D**) Risk scores for each sample and mean of risk scores (solid black line). **E**) Stacked chart of the proportions of different cell types within the low- and high-risk groups. **F**-**H**) bar plot and dimensional reduction plot displaying the expression patterns of SLC25A38 (**F**), EDNRB (**G**) and LURAP1 (**H**)

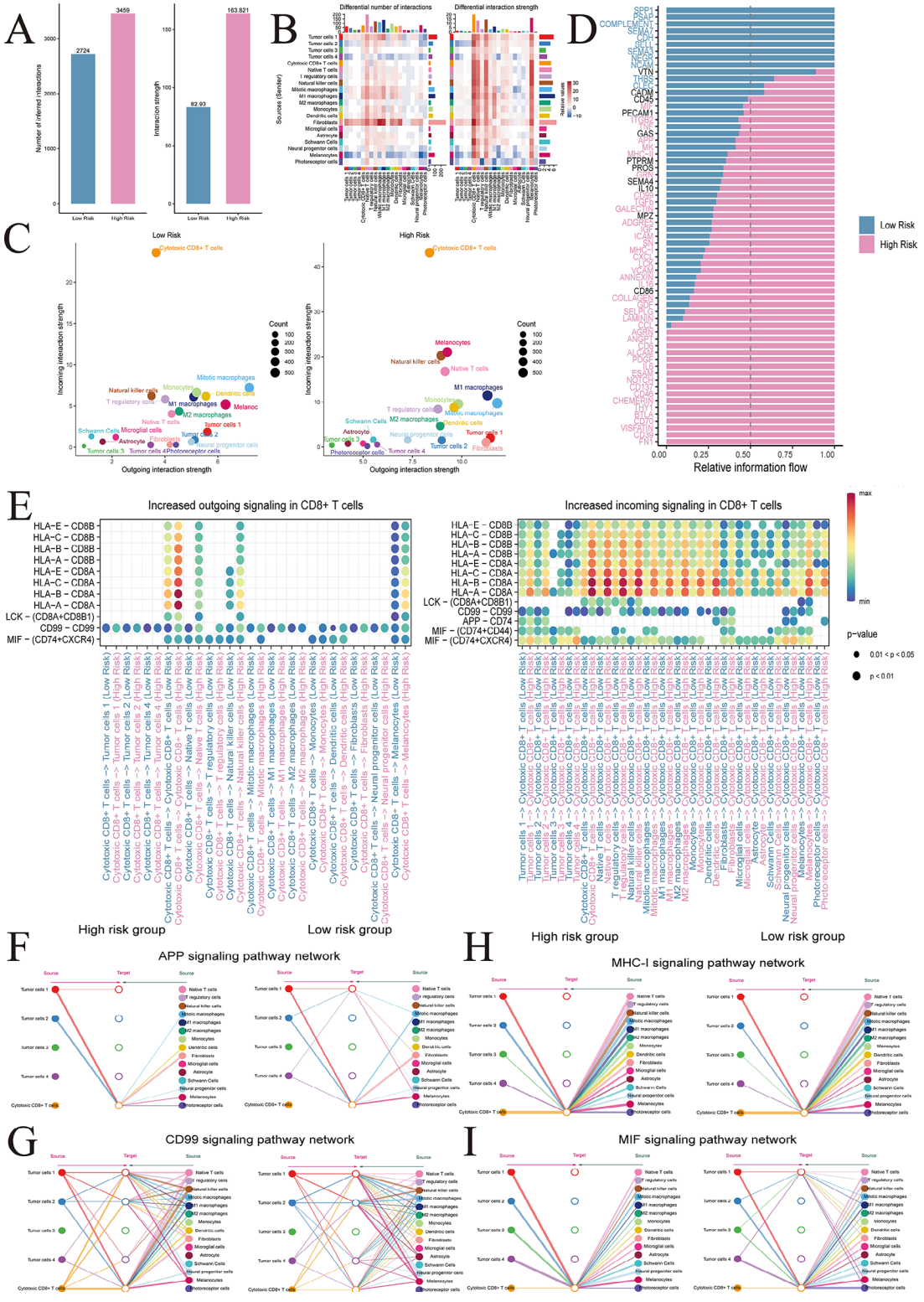

Fig. 7 CD8 + T cells play an important role in cellular communication **A**) Bar graph illustrating the quantity and strength of cell communication between the low- and high-risk groups. **B**) Heatmap of the quantity and strength of cell communication among different cell types in the low- and high-risk groups. **C**) Scatter plot representing the relative strength of cell communication for each cell type. **D**) Cellular communication pathways significantly different between the two groups. **E**) Bubble plot of ligand receptor expression for pathways associated with cytotoxic CD8 + T cells. **F**-**I**) Hierarchical plots demonstrating cytotoxic CD8 + T cells -associated pathways significantly upregulated in high-risk groups: the APP pathway (**F**), the MHC-I pathway (**H**), the CD99 pathway (**G**), and the MIF pathway (**I**)

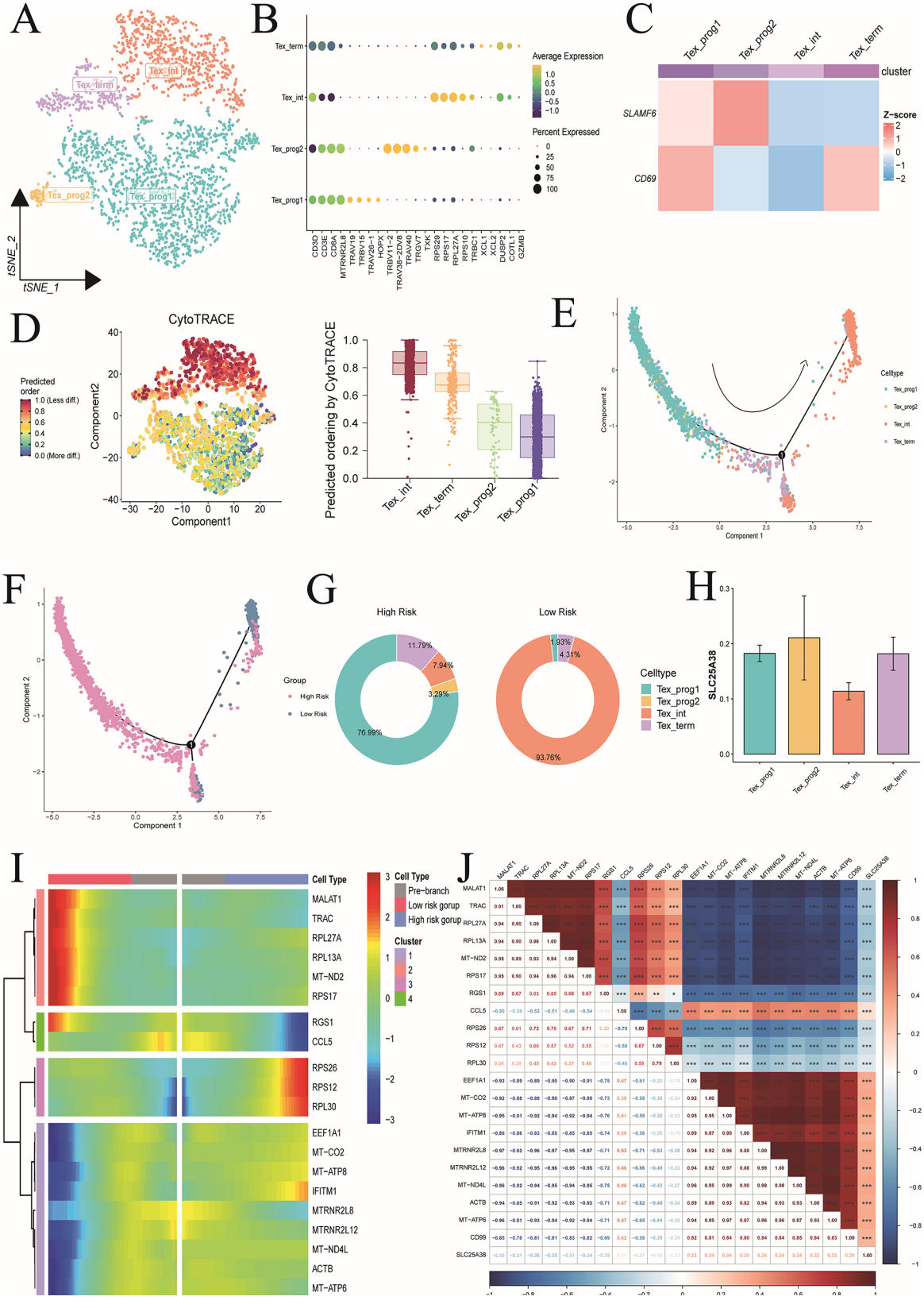

Fig. 8 (See legend on next page.)

(See figure on previous page.)

Fig. 8 Exploring the differentiation trajectory of $CD8^+$ T cells **A**) tSNE was utilized as a dimensionality reduction technique to project a reclustered Seurat clustering system of cytotoxic CD8 + T cells. **B**) Bubble plot of cytotoxic CD8 + T cells subsets marker genes.**C**) Heatmap of T cell exhaustion marker expression in CD8 + T cell subsets.**D**) Dimplot(left) and box plot(right) demonstrating CytoTRACE scores of CD8 + T cell subsets. **E** and **F**) Pseudotime trajectory analysis showing cytotoxic CD8 + T cells subsets. The cells are coloured according to cell type (**E**) and group (**F**). G)Doughnut plot showing the percentage of each T-cell subsets seen in the two groups. **H**) Bar plot demonstrating the expression of SLC25A38 among various subsets of T cells. **I**) Heatmap of genes associated with cytotoxic CD8 + T cells cell differentiation by BEAM analysis. **J**) Heatmap of correlation between differentiation-related genes and prognostic biomarker SLC25A38

each subtype in the two groups, and found that the T cells in the high-risk group were predominantly Tex_prog1 and Tex_term, while those in the low-risk group were predominantly Tex_int (Fig. 8G). We calculated the expression of SLC25A38 in various subtypes of T cells and found that SLC25A38 expression was lowest in Tex_int (Fig. 8H). We then identified 20 genes associated with cytotoxic CD8+ T cells differentiation by BEAM analysis (Fig. 8I). Finally, the correlation between the prognostic biomarker SCL25A38 expressed in T cells and these differentiation-related genes was calculated. SLC25A38 was significantly associated with those genes (Fig. 8J).

Discussion

In this study, we constructed a prognostic model containing three genes by a machine learning approach. And the validity and robust of the model was verified in the external dataset of the internal dataset. After that, the prognostic biomarkers in the model were validated by cellular experiments, and it was found that these three genes regulate tumor metastasis by modulating the migration of tumor cells rather than affecting tumor proliferation or apoptosis. Then by immune infiltration analysis, CD8+ T cells were found to play an important role in this process. Finally, the specific function of CD8+ T cells in the immune microenvironment was further explored using single-cell transcriptomic data.

Differential gene expression analysis is a crucial tool for understanding cancer prognosis [27]. Studies utilizing DNA methylation and gene expression data have identified genes that provide prognostic insights into overall survival and metastatic risk in UM [28–30]. Our findings align with previous research, which indicated that specific immune cell populations are linked to overall survival in UM [31,32]. Integrating immunological data with clinical and pathological information has shown promising results, achieving an AUC of approximately 0.8 in survival predictions. Additionally, neural networks have been employed to assess melanoma prognosis based on patient demographics and tumor characteristics [33]. These models have estimated a 5-year survival rate for UM patients with tumors as high as 84% [34]. Notably, our predictive model features a relatively small number of genes compared to existing models, yet it achieves an impressive AUC of 0.95 for predicting survival. This work allows for a deeper discussion of the mechanisms underlying metastasis and provides insights into the tumor immune microenvironment.

In the present study prognostic biomarkers were all able to promote the migration of tumor cells and thus influence the prognosis of patients. Meanwhile, previous studies have reported that the three genes included in the prognostic model developed in this study have key regulatory roles in a variety of physiopathological processes. SLC25A38 protein belongs to the SLC25 family of mitochondrial carrier proteins [35]. SLC25A38 has been reported to be involved in heme synthesis in eukaryotes as a glycine trans-mitochondrial transporter. The early research on it focused on anemia [36–38]. SLC25A38 acts as a transporter of glycine in the inner mitochondrial membrane, inhibition of SLC25A38 may inhibit glycine transport to the cytoplasm and lead to accumulation of glycine in mitochondria. Glycine metabolism and expression of the mitochondrial glycine biosynthetic pathway are closely associated with the proliferation rate of cancer cells [39]. It can be speculated that SLC28A38 has a potential role in the proliferation and migration of cancer cells. This has been demonstrated in some recent studies [9,40]. A recent study found that SLC25A38 plays an important role in the metastasis of UM [9], which is consistent with our findings. EDNRB is non-specific receptor for endothelin 1, 2, and 3. Mediates its action by association with G proteins that activate a phosphatidylinositol-calcium second messenger system [41]. Recently, evidence has shown that EDNRB plays an important role in the development of many cancers such as lung cancer, glioma, breast cancer and colorectal cancer [41]. LURAP1 involved in positive regulation of I-kappaB kinase/NF-kappaB signaling and positive regulation of cytokine production [42]. Some studies have demonstrated its importance in cell movements [42]. Although a study has been conducted to incorporate LURAP1 into prognostic models of bladder tumors [43], its role in tumors has not been fully elucidated.

To further explore the mechanisms of this prognostic model, we focused our attention on the immune microenvironment. Many previous studies have demonstrated the critical role of the immune microenvironment in tumor initiation, proliferation, and metastasis. The immune system not only suppresses melanoma occurrence and progression, but also depending on the tumor microenvironment, can promote tumor development through interactions with immune cells [44]. T cells

are the most infiltrating immune cells in the melanoma microenvironment, and higher infiltration often indicates a better prognosis for melanoma [45]. CD8+T cells specifically influence melanoma sensitivity to immunotherapy and their expression of immune checkpoint receptors such as anti-CTLA-4 and PD-1 antibodies are crucial for advanced melanoma treatment, including in cases of melanoma brain metastases [46].

In this study, CD8+ T cells were found to infiltrate significantly more in the metastasis high-risk group than in the low-risk group, suggesting that it may play a key role in the process of UM metastasis. We found that CD8+ T cells play a very important role in cellular communication in the UM microenvironment. Also in the high metastasis risk group CD8+ T cell communication was significantly upregulated. Among the pathways we identified, only the CD99 pathway is signaling from CD8+T cells to tumor cells, and CD99 pathway may be a key pathway to promote UM metastasis. Numerous previous studies have found that CD99 promotes the progression of hematologic tumors and Ewing's Sarcoma [47–49].CD99 increases cell viability, colony formation and cell migration in leukemia cell lines and primary leukemia cells [47]. Both the eye and the bone marrow are immune-privileged, and their metastatic processes are both processes in which the tumor is re-exposed to the immune system. Thus, the mechanisms by which CD99 affects tumor cell migration may be similar. CD99 is expressed in about 60% of primary cutaneous melanomas [50],making it a useful marker for differentiating between spitzoid melanoma and Spitz nevus [51]. However, research on CD99 in melanoma is limited. Our study found that the CD99 signaling pathway may plays an important role in cell communication between CD8+T cells and tumors. The MHC-I pathway of the remaining three pathways is likely to be associated with UM antigen exposure. In many malignancies, tumor cells lose expression of one or more HLA alleles, thereby evading T cell-mediated immune responses [52]. However, due to the immune privilege of the eye, HLA antigens of UM are not exposed to the immune system in the absence of metastasis. Upregulation of the MHC-I pathway in the high metastasis risk group is likely to be associated with early metastasis. The MHC-I-mediated antigenic peptide presentation pathway is crucial for anticancer immunity, with the deletion or down-regulation of MHC-I serving as a primary mechanism for tumor escape [53]. Research indicates that the BRAF V600E mutation, the most prevalent activating kinase mutation in melanoma, leads to the rapid internalization of MHC-I from the melanoma cell surface, resulting in its accumulation in the endolysosomal compartment [54]. Despite this, MAPK inhibitors have shown limited effectiveness in clinical trials involving UM patients, suggesting that the MAPK pathway may play a paracrine role in tumor development [15]. Moreover, immunopositivity for BRAFV600E in intraocular melanoma supports its association with metastatic disease [55]. Amyloid precursor protein (APP), typically linked to Alzheimer's disease, has been found to influence metastatic melanoma cell proliferation. Blocking APP expression not only reduces the growth of these cells but also increases their sensitivity to various chemotherapeutic agents. Targeting APP may thus offer a promising strategy for melanoma treatment, particularly in UM metastasis [56]. Macrophage migration inhibitory factor (MIF) is a multifunctional pro-inflammatory protein that acts as an immunomodulator [57], promoting inflammation associated with tumor growth and metastasis across several cancers [58]. In pancreatic cancer, for instance, MIF's tautomerase inhibitor IPG1576 has been shown to inhibit myeloid-derived suppressor cell differentiation and reduce tumor growth, coinciding with increased infiltration of CD8+T cells in the tumor microenvironment. This mechanism parallels our findings and underscores the broader research potential of IPG1576 [60,61].

Finally, we initially explored the differentiation and heterogeneity of CD8+ T cells in UM. CD8+T cells are pivotal in anticancer immunotherapy. Yet, persistent antigen exposure and inflammatory stimuli can lead to diminished proliferation and effector function, resulting in a state known as CD8+T cell exhaustion (Tex) [61]. Exhausted CD8+T cells cells in tumors occupy distinct ecological niches that influence transcriptional processes during intercellular state transitions [62]. Understanding the molecular and epigenetic mechanisms governing the various phases of Tex may reveal new opportunities for cancer immunotherapy [25]. Although our study seemed to obtain the result that CD8+T cell infiltration made the prognosis worse in the Bulk-rna seq data analysis section, in the follow-up single-cell transcriptome sequencing data section we found that although the number of CD8+T cells was increased in the high metastatic risk group, most of these T cells were exhausted state T cells and progenitor T cells. The increase in the number of T cells was most likely due to impaired in the function of the T cells, and resulted in a compensatory increase. This provides a promising therapeutic direction for immunotherapy in UM - prevention of T cell exhaustion.

We are looking forward to more studies in the future to elucidate the role of CD8+ T cells in UM metastasis.

In this study, we developed a stable prognostic model for predicting the risk of metastasis and prognosis of UM patients, and also found that CD8+ T in the tumor

microenvironment plays a key role in the metastatic process of UM.

Supplementary Information

The online version contains supplementary material available at https://doi.org/10.1186/s12935-024-03539-3.

Supplementary Material 1: Supplementary Table 1： Statistical charts of database patient information 2. Figure S1: Cell viability assay, Quantitative real-time PCR and apoptosis flow assays

Acknowledgements
We thank the participants and researchers at GEO providing publicly available data.

Author contributions
S. Chen and Z. Tang designed this research. S. Chen, Q. Wang, W. Huang and X. Li collected the public datasets. S. Chen, Z. Tang, X. Li, W. Huang and X. Huang performed the bioinformatic analyses. Y. Chen, Z. Tang, and S. Zheng conducted the experiments. S. Chen, Z. Tang, J. Wu, C. Lu and Q. Wang contributed to the statistical analyses. S. Chen and Z. Tang wrote the article. All the authors participated in planning, execution, and analysis and read and approved the final submitted version.

Funding
This work was supported by the Natural Science Foundation of Hunan Province (NO. 2023JJ30770 and 2023JJ60137), the National Natural Science Foundation of China (No. 82000924), the General Undergraduate Colleges and Universities Teaching Reform Research Project of Hunan Province (NO. 2024 – 223), the Educational Reform Project of Central South University (NO.2024jy067) and Scientific Research Program Projects of Hunan Provincial Health Commission (NO. 202207022525).

Data availability
No datasets were generated or analysed during the current study.

Declarations

Ethics approval and consent to participate
As previously collected and published data were reanalyzed, no further ethical approval was needed.

Consent for publication
All the authors read the final version and approved it.

Institutional review board statement
Not applicable.

Competing interests
The authors declare no competing interests.

Author details
[1]Department of Ophthalmology, The Second Xiangya Hospital, Central South University, Changsha 410011, China
[2]Hunan Clinical Research Center of Ophthalmic Disease, Changsha, Hunan 410011, China
[3]Department of Anaesthesiology, The Second Xiangya Hospital, Central South University, Changsha 410011, China
[4]Hunan Centre for Drug Review and Adverse Reaction Monitoring, Changsha, Hunan 410013, China
[5]Hunan Provincial Drug Administration, Changsha, Hunan 410013, China
[6]Hunan Provincial Key Laboratory of Critical Quality Attribute of Cell Therapy Products, Changsha, Hunan 410013, China

Received: 19 July 2024 / Accepted: 17 October 2024
Published online: 30 October 2024

References

1. Amaro A, Gangemi R, Piaggio F et al. The biology of uveal melanoma. CANCER METAST REV. 2017 2017-3-1;36(1):109–40.
2. Kujala E, Mäkitie T, Kivelä T. Very long-term prognosis of patients with malignant uveal melanoma. INVEST OPHTH VIS SCI. 2003 2003-1-1;44(11):4651.
3. Shields CL, Kaliki S, Furuta M, Fulco E, Alarcon C, Shields JA. American Joint Committee on Cancer Classification of Uveal Melanoma (Anatomic Stage) Predicts Prognosis in 7731 Patients: The 2013 Zimmerman Lecture. OPHTHALMOLOGY. 2015 2015-1-1;122(6):1180-6.
4. Krantz BA, Dave N, Komatsubara KM, Marr BP, Carvajal RD. Uveal melanoma: epidemiology, etiology, and treatment of primary disease. CLIN OPHTHALMOL. 2017 2017-1-20;11:279 – 89.
5. Berus T, Halon A, Markiewicz A, Orlowska-Heitzman J, Romanowska-Dixon B, Donizy P. Clinical, histopathological and cytogenetic prognosticators in Uveal Melanoma - A Comprehensive Review. ANTICANCER RES. 2017 2017-12-1;37(12):6541–9.
6. Shields CL, Furuta M, Thangappan A et al. Metastasis of uveal melanoma millimeter-by-millimeter in 8033 consecutive eyes. Arch Ophthalmol. 2009 2009-8-1;127(8):989 – 98.
7. Shields CL, Say EAT, Hasanreisoglu M et al. Cytogenetic Abnormalities in Uveal Melanoma Based on Tumor Features and Size in 1059 Patients: The 2016 W. Richard Green Lecture. OPHTHALMOLOGY. 2017 2017-1-1;124(5):609 – 18.
8. Kilic E, van Gils W, Lodder E et al. Clinical and cytogenetic analyses in uveal melanoma. INVEST OPHTH VIS SCI. 2006 2006-9-1;47(9):3703–7.
9. Fan Z, Duan J, Luo P et al. SLC25A38 as a novel biomarker for metastasis and clinical outcome in uveal melanoma. CELL DEATH DIS. 2022 2022-1-1;13(4):330.
10. Field MG, Decatur CL, Kurtenbach S et al. PRAME as an independent biomarker for Metastasis in Uveal Melanoma. CLIN CANCER RES. 2016 2016-3-1;22(5):1234–42.
11. Schoenfield L, Janse S, Kline D et al. Estrogen Receptor Is Expressed in Uveal Melanoma: A Potential Target for Therapy. OCUL ONCOL PATHOL. 2021 2021-9-1;7(4):303 – 10.
12. Meng Z, Chen Y, Wu W et al. PRRX1 is a Novel Prognostic Biomarker and facilitates Tumor Progression through epithelial-mesenchymal transition in Uveal Melanoma. FRONT IMMUNOL. 2022 2022-1-1;13:754645.
13. Onken MD, Worley LA, Tuscan MD, Harbour JW. An Accurate, clinically feasible Multi-gene expression assay for Predicting Metastasis in Uveal Melanoma. The Journal of molecular diagnostics: JMD. 2010 2010-1-1;12(4):461–8.
14. Onken MDMD, Worley LALA, Char DHDH et al. Collaborative Ocular Oncology Group Report No. 1: Prospective Validation of a Multi-Gene Prognostic Assay in Uveal Melanoma. Ophthalmology (Rochester, Minn.). 2012 2012-1-1;119(8):1596 – 603.
15. Jager MJ, Shields CL, Cebulla CM et al. Uveal melanoma. NAT REV DIS PRIMERS. 2020 2020-4-9;6(1):24.
16. Thorsson V, Gibbs DL, Brown SD et al. The Immune Landscape of Cancer. IMMUNITY. 2018 2018-4-17;48(4):812–30.
17. Colli LM, Machiela MJ, Myers TA, Jessop L, Yu K, Chanock SJ. Burden of nonsynonymous mutations among TCGA Cancers and candidate Immune Checkpoint inhibitor responses. CANCER RES. 2016 2016-7-1;76(13):3767–72.
18. Tobal K, Deuble K, McCartney A, Lightman S. Characterization of cellular infiltration in choroidal melanoma. MELANOMA RES. 1993 1993-2-1;3(1):63 – 5.
19. Chen Y, Xu H, Xu H, et al. Exploration of diagnostic biomarkers, microenvironment characteristics, and ursolic acid's therapeutic effect for benign prostate hyperplasia. INT J BIOL SCI. 2023;19(13):4242–58.
20. Chen S, Huang W, Wan Q, et al. Investigation of the acute pathogenesis of spondyloarthritis/HLA-B27-associated anterior uveitis based on genome-wide association analysis and single-cell transcriptomics. J TRANSL MED. 2024;22(1):271. 2024-3-12.
21. Sheng B, Pan S, Ye M et al. Single-cell RNA sequencing of cervical exfoliated cells reveals potential biomarkers and cellular pathogenesis in cervical carcinogenesis. CELL DEATH DIS. 2024 2024-1-1;15(2):130.
22. Yoshihara K, Shahmoradgoli M, Martinez E, et al. Inferring tumour purity and stromal and immune cell admixture from expression data. NAT COMMUN. 2013;2013–1–20:4:2612.
23. Li B, Severson E, Pignon J, et al. Comprehensive analyses of tumor immunity: implications for cancer immunotherapy. GENOME BIOL. 2016;2016–1–1(1):174.
24. Sturm G, Finotello F, Petitprez F et al. Comprehensive evaluation of transcriptome-based cell-type quantification methods for immuno-oncology. Bioinformatics. 2019 2019-7-15;35(14):i436–45.

25. Beltra JC, Manne S, Abdel-Hakeem MS et al. Developmental Relationships of Four Exhausted CD8(+) T Cell Subsets Reveals Underlying Transcriptional and Epigenetic Landscape Control Mechanisms. IMMUNITY. 2020 2020-5-19;52(5):825 – 41.
26. Gulati GS, Sikandar SS, Wesche DJ et al. Single-cell transcriptional diversity is a hallmark of developmental potential. SCIENCE. 2020 2020-1-24;367(6476):405 – 11.
27. Chandrabhatla AS, Horgan TM, Cotton CC, Ambati NK, Shildkrot YE. Clinical applications of machine learning in the management of intraocular cancers: a narrative review. INVEST OPHTH VIS SCI. 2023 2023-7-3;64(10):29.
28. Chi H, Peng G, Yang J et al. Machine learning to construct sphingolipid metabolism genes signature to characterize the immune landscape and prognosis of patients with uveal melanoma. FRONT ENDOCRINOL. 2022 2022-1-20;13:1056310.
29. Lv X, Ding M, Liu Y. Landscape of Infiltrated Immune Cell characterization in Uveal Melanoma to Improve Immune Checkpoint Blockade Therapy. FRONT IMMUNOL. 2022 2022-1-20;13:848455.
30. Hou P, Bao S, Fan D et al. Machine learning-based integrative analysis of methylome and transcriptome identifies novel prognostic DNA methylation signature in uveal melanoma. BRIEF BIOINFORM. 2021 2021-7-20;22(4).
31. Eason K, Nyamundanda G, Sadanandam A. polyClustR: defining communities of reconciled cancer subtypes with biological and prognostic significance. BMC BIOINFORMATICS. 2018 2018-5-25;19(1):182.
32. Wang T, Wang Z, Yang J, Chen Y, Min H. Screening and identification of key biomarkers in metastatic uveal melanoma: evidence from a bioinformatic analysis. J CLIN MED. 2022 2022-12-5;11(23).
33. Zhang Z, Ni Y, Chen G, Wei Y, Peng M, Zhang S. Construction of immune-related risk signature for uveal melanoma. ARTIF CELL NANOMED B. 2020 2020-12-1;48(1):912–9.
34. Kaiserman I, Rosner M, Pe'Er J. Forecasting the prognosis of choroidal melanoma with an artificial neural network. Ophthalmology. 2005 2005-9-1;112(9):1608.
35. Haitina T, Lindblom J, Renström T, Fredriksson R. Fourteen novel human members of mitochondrial solute carrier family 25 (SLC25) widely expressed in the central nervous system. GENOMICS. 2006 2006-1-1;88(6):779 – 90.
36. Uminski K, Houston DS, Hartley JN, Liu J, Cuvelier GDE, Israels SJ. Clinical characterization and hematopoietic stem cell transplant outcomes for congenital sideroblastic anemia caused by a novel pathogenic variant in SLC25A38. PEDIATR BLOOD CANCER. 2020 2020-1-1;67(10):e28623.
37. Bottomley SS, Campagna DR, Matsuoka M, et al. Mutations in mitochondrial carrier family gene SLC25A38 cause nonsyndromic autosomal recessive congenital sideroblastic anemia. NAT GENET. 2009;2009–1–1(6):651–3.
38. Heeney MM, Berhe S, Campagna DR et al. SLC25A38 congenital sideroblastic anemia: phenotypes and genotypes of 31 individuals from 24 families, including 11 novel mutations, and a review of the literature. HUM MUTAT. 2021 2021-1-1;42(11):1367–83.
39. Jain M, Nilsson R, Sharma S, et al. Metabolite profiling identifies a key role for glycine in rapid cancer cell proliferation. Science. 2012;336(6084):1040–4. 2012-5-25.
40. CHEN H, LU Q, ZHANG Y, ZHANG C, ZHANG H. Overexpression of SLC25A38 protein on acute lymphoblastic leukemia cells. ONCOL LETT. 2014;2014–1–1(5):1422–6.
41. Webb ML, Chao CC, Rizzo M et al. Cloning and expression of an endothelin receptor subtype B from human prostate that mediates contraction. MOL PHARMACOL. 1995 1995-4-1;47(4):730–7.
42. Jing Z, Yuan X, Zhang J, et al. Chromosome 1 open reading frame 190 promotes activation of NF-kappaB canonical pathway and resistance of dendritic cells to tumor-associated inhibition in vitro. J IMMUNOL. 2010;185(11):6719–27. 2010-12-1.
43. Wang L, Shi J, Huang Y et al. A six-gene prognostic model predicts overall survival in bladder cancer patients. CANCER CELL INT. 2019 2019-1-20;19:229.
44. Tower H, Ruppert M, Britt K. The Immune Microenvironment of breast Cancer progression. CANCERS. 2019 2019-9-16;11(9).
45. Edwards J, Tasker A, Pires DSI et al. Prevalence and Cellular distribution of Novel Immune checkpoint targets across longitudinal specimens in Treatment-naïve Melanoma patients: implications for clinical trials. CLIN CANCER RES. 2019 2019-6-1;25(11):3247–58.
46. Carlino MS, Larkin J, Long GV. Immune checkpoint inhibitors in melanoma. LANCET. 2021 2021-9-11;398(10304):1002–14.
47. Vaikari VP, Du Y, Wu S et al. Clinical and preclinical characterization of CD99 isoforms in acute myeloid leukemia. HAEMATOLOGICA. 2020 2020-4-1;105(4):999–1012.
48. Huijbers E, van der Werf IM, Faber LD et al. Targeting Tumor Vascular CD99 inhibits Tumor Growth. FRONT IMMUNOL. 2019 2019-1-20;10:651.
49. Chung SS, Eng WS, Hu W et al. CD99 is a therapeutic target on disease stem cells in myeloid malignancies. SCI TRANSL MED. 2017 2017-1-25;9(374).
50. Wilkerson AE, Glasgow MA, Hiatt KM. Immunoreactivity of CD99 in invasive malignant melanoma. J CUTAN PATHOL. 2006 2006-10-1;33(10):663–6.
51. King MS, Porchia SJ, Hiatt KM. Differentiating spitzoid melanomas from Spitz nevi through CD99 expression. J CUTAN PATHOL. 2007 2007-7-1;34(7):576–80.
52. Garrido F, Algarra I. MHC antigens and tumor escape from immune surveillance. ADV CANCER RES. 2001 2001-1-20;83:117 – 58.
53. Wu X, Li T, Jiang R, Yang X, Guo H, Yang R. Targeting MHC-I molecules for cancer: function, mechanism, and therapeutic prospects. MOL CANCER. 2023;22(1):194. 2023-12-2.
54. Bradley SD, Chen Z, Melendez B et al. BRAFV600E co-opts a conserved MHC class I internalization pathway to Diminish Antigen Presentation and CD8 + T-cell Recognition of Melanoma. CANCER IMMUNOL RES. 2015 2015-6-1;3(6):602–9.
55. Neerukonda VK, Kim IK, Stagner AM. Primary vitreoretinal involvement and immunopositivity for BRAFV600E help distinguish metastatic from primary intraocular melanoma: a detailed histopathologic study of metastatic cutaneous melanoma to the eye. HISTOPATHOLOGY. 2022 2022-6-1;80(7):1061–70.
56. Botelho MG, Wang X, Arndt-Jovin DJ, Becker D, Jovin TM. Induction of terminal differentiation in melanoma cells on downregulation of beta-amyloid precursor protein. J INVEST DERMATOL. 2010 2010-5-1;130(5):1400–10.
57. Sumaiya K, Langford D, Natarajaseenivasan K, Shanmughapriya S. Macrophage migration inhibitory factor (MIF): A multifaceted cytokine regulated by genetic and physiological strategies. PHARMACOL THERAPEUT. 2022 2022-5-1;233:108024.
58. O'Reilly C, Doroudian M, Mawhinney L, Donnelly SC. Targeting MIF in Cancer: therapeutic strategies, current developments, and Future opportunities. MED RES REV. 2016 2016-5-1;36(3):440–60.
59. Yan L, Wu M, Wang T et al. Breast Cancer stem cells secrete MIF to mediate Tumor metabolic reprogramming that drives Immune Evasion. CANCER RES. 2024 2024-4-15;84(8):1270–85.
60. Jia X, Xi J, Tian B et al. The tautomerase activity of Tumor Exosomal MIF promotes pancreatic Cancer Progression by modulating MDSC differentiation. CANCER IMMUNOL RES. 2024 2024-1-3;12(1):72–90.
61. Wang Q, Qin Y, Li B. CD8(+) T cell exhaustion and cancer immunotherapy. CANCER LETT. 2023 2023-4-10;559:216043.
62. Dolina JS, Van Braeckel-Budimir N, Thomas GD, Salek-Ardakani S. CD8(+) T cell exhaustion in Cancer. FRONT IMMUNOL. 2021 2021-1-20;12:715234.

Publisher's note